

Supporting information:

Driving forces for the phase transition of CuQ₂-TCNQ molecular crystals

Dehong Yu*, Gordon J. Kearley, Guangfeng Liu, Richard A. Mole, Xutang Tao*

Contents:

Experimental Section

Simulation

Figure S1. Temperature dependent generalized phonon density of states (GDOS) for form-II CuQ₂-TCNQ

Figure S2. Temperature dependent generalized phonon density of states (GDOS) for form-I CuQ₂-TCNQ.

Figure S3. Comparison of GDOS between Form-I and Form-II CuQ₂-TCNQ at three temperatures: 100 K, 200 K and 400 K.

Figure S4. Hirshfeld surface of CuQ₂-TCNQ: Form-I (left) and Form-II (right). The view is along the crystallorgraphic *a*-axis.

Figure S5. Fingerprint plots for Form-I and Form-II CuQ₂-TCNQ resolved into individual atomic contacts.

Table S1. Relative contributions to the Hirshfeld surface area for the various close intermolecular contacts for Form-I and Form-II CuQ₂-TCNQ

References.

Experimental Section:

Sample preparation

A mixture of bis-(8-hydroxyquinolinato) copper (II), CuQ₂, (10.0 mg) and tetracyanoquinodimethane, TCNQ, (5.8 mg) with a molar ratio 1:1 was dispersed in 10 mL chloroform using an ultrasonic bath for 30 min. After ultrasonic treatment, the solution was filtered into a 20 mL conical flask through a micro-pore film and left for slow solvent evaporation under ambient conditions for about 5 to 6 days. Then micron-grade single crystals of form-II were formed and the structure was characterized by X-ray diffraction (XRD). For neutron spectroscopy measurements, the as-grown form-II was used. It is noted that temperature variation from 100 K to 400 K in a standard closed cycle refrigerator/heater was only able to induce the transition from form-II to form-I for a small percentage of the sample, this being determined by XRD analysis. Simply grinding form-II sample did not induce complete phase transition either. This is most likely due to the broad size distribution of the as-grown form-II sample. Finally, the form-I powder sample for neutron measurements was obtained by applying a pressure of 600 MPa to form-II, followed by grinding. XRD confirmed that the pressed sample was 90% in the form-I structure.

Neutron Scattering

Inelastic neutron scattering (INS) experiments were conducted on the time-of-flight cold neutron spectrometer, Pelican, at the Bragg Institute, Australian Nuclear Science and Technology Organisation^{s1,s2}. The powder samples were placed in an annular aluminium can and attached to the cold head of a closed-cycle refrigerator capable of achieving sample temperature from 4 K to 400 K. The wavelength of the incident neutrons was 4.75 Å corresponding to an energy of 3.63 meV. The Large Array Manipulation Program (LAMP)^{s3} was used to reduce the data and convert the time-of-flight data to $S(Q, \omega)$ – the scattering function which contains the dynamic information of the system. Background subtraction of the empty sample can and normalisation to vanadium sample for correcting detector efficiency was also made. Finally the scattering function was converted to the generalised phonon density of states (GDOS)^{s4} as a function of energy transfer at the neutron-energy-gain-side. The GDOS has accounted for the temperature dependence of the $S(Q, \omega)$ related to the thermal

population of excitations. Any temperature dependence of the GDOS would be an indication of deviation from harmonic motion of the molecular dynamics of the system. The 10% form-II contribution to the form-I data has been subtracted, though it barely affected the result.

Density functional theory (DFT) calculations were carried out using the plane-wave code, Vienna Ab-initio Simulation Package (VASP)^{s5,s6}. Geometry optimisation and MD simulations were performed using the Projector Augmented Wave (PAW)^{s7} potential and the Perdew-Burke-Ernzerhof (PBE)^{s8} exchange-correlation functional. For geometry optimisations a 4 x 4 x 3 Γ -centered Monkhorst-Pack^{s9} k-point mesh and 400 eV energy cutoff were used. Geometry and unit-cell optimisations were achieved by allowing the atoms to relax to their minimum energy positions, with the cell constants being successively refined in separate optimisations. An electronic-energy convergence of 1.0×10^{-5} eV was ensured for these calculations. The MD simulations were made using a single k-point (Γ -point). An energy cutoff of 300 eV and electronic-energy convergence of 1.0×10^{-4} eV were used in the MD simulations. After the structure optimisations, a 17 ps simulation with 1 fs time step under isokinetic ensemble (NVT) was carried out to ensure a correct energy distribution, followed by a 17ps production run in the microcanonical (NVE) ensemble. The MD trajectories were used to calculate the INS spectrum using nMoldyn^{s10}. This was achieved via the incoherent intermediate scattering function $F(Q,t)$ that was calculated on a regular grid in both momentum transfer Q and time t . These values were then Fourier transformed to obtain the scattering function $S(Q,\omega)$. The appropriate cut in Q was taken to coincide with the experimental INS spectrum on Pelican instrument at ANSTO.

Hirshfeld isoelectric surfaces for Form-I and Form-II $\text{CuQ}_2\text{-TCNQ}$ have been generated using Crystal Explorer^{s11}. Wavefunction calculations were performed using Tonto program with STD-3G molecular basis. 2D fingerprint plots were displayed with the standard view option covering di and de distance from 0.6 to 2.6 Å, where di and de are the distances from the surface to the nearest atoms, interior and exterior to the surface, respectively^{s12}.

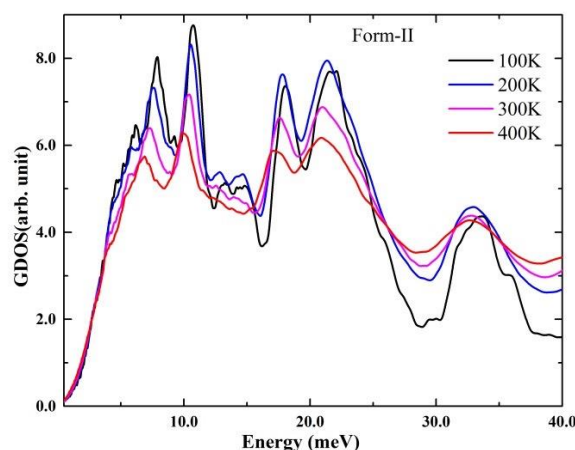


Figure S1. Temperature dependent generalized phonon density of states (GDOS) for form-II $\text{CuQ}_2\text{-TCNQ}$

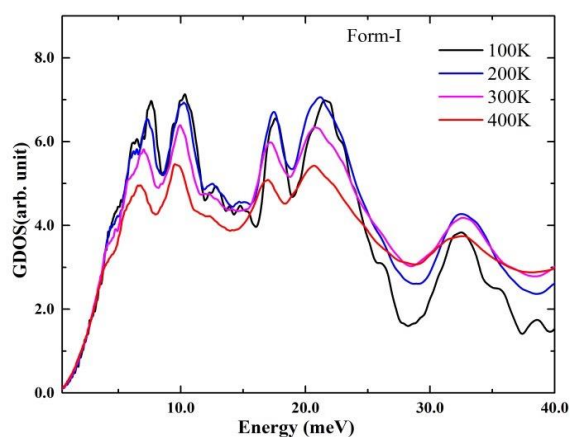


Figure S2. Temperature dependent generalized phonon density of states (GDOS) for form-I $\text{CuQ}_2\text{-TCNQ}$.

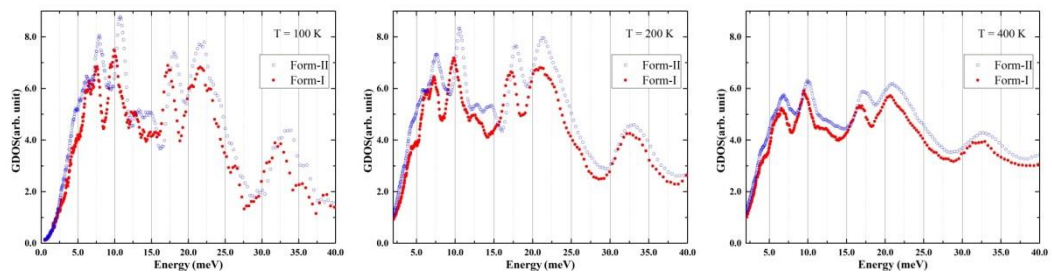


Figure S3. Comparison of GDOS between form-I and form-II $\text{CuQ}_2\text{-TCNQ}$ at three temperatures: 100 K, 200 K and 400 K.



Figure S4. Hirshfeld surface of CuQ₂-TCNQ: form-I (left) and form-II (right). The view is along the crystallographic *a*-axis.

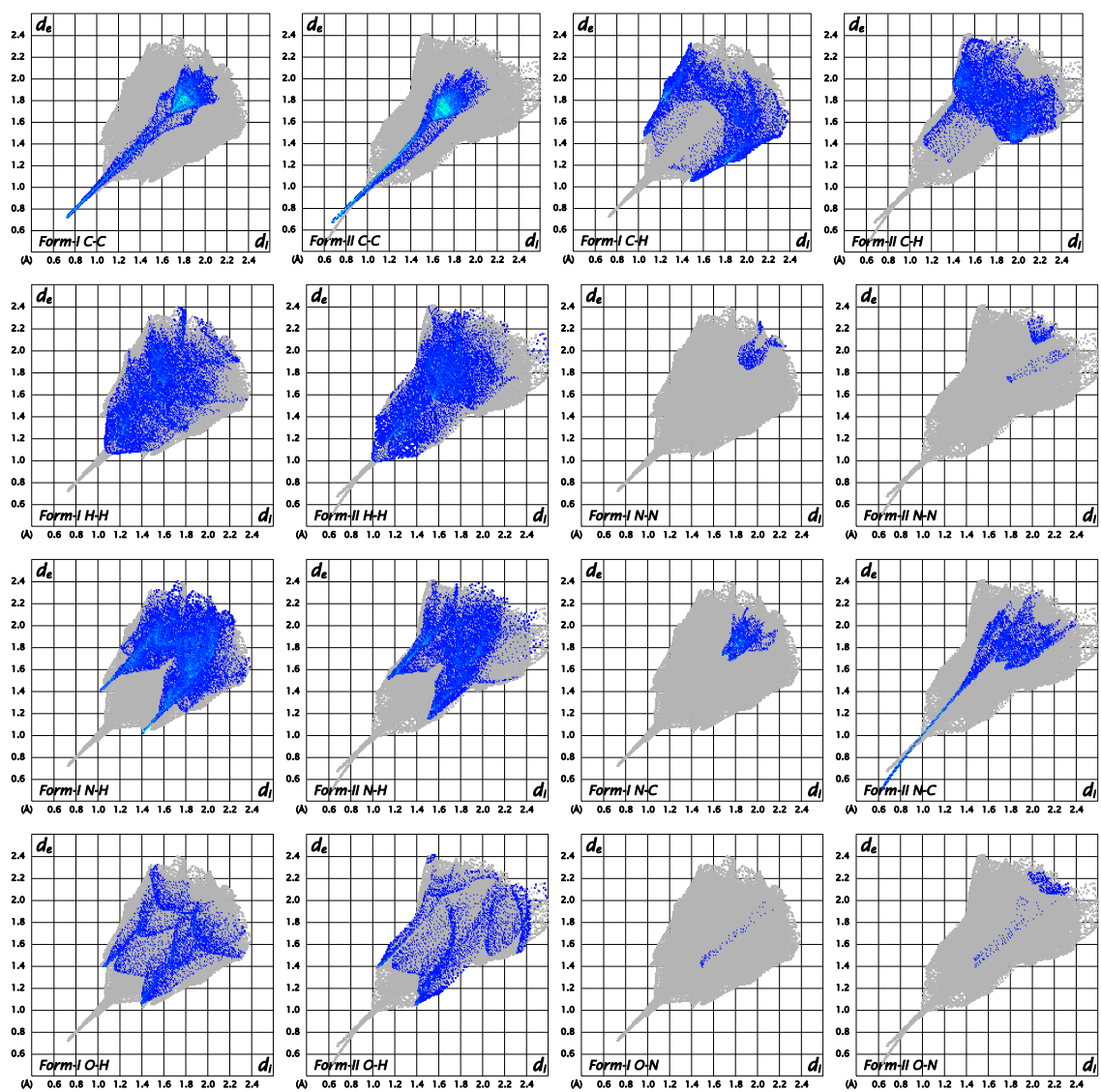


Figure S5. Fingerprint plots for form-I and form-II $\text{CuQ}_2\text{-TCNQ}$ resolved into individual atomic contacts.

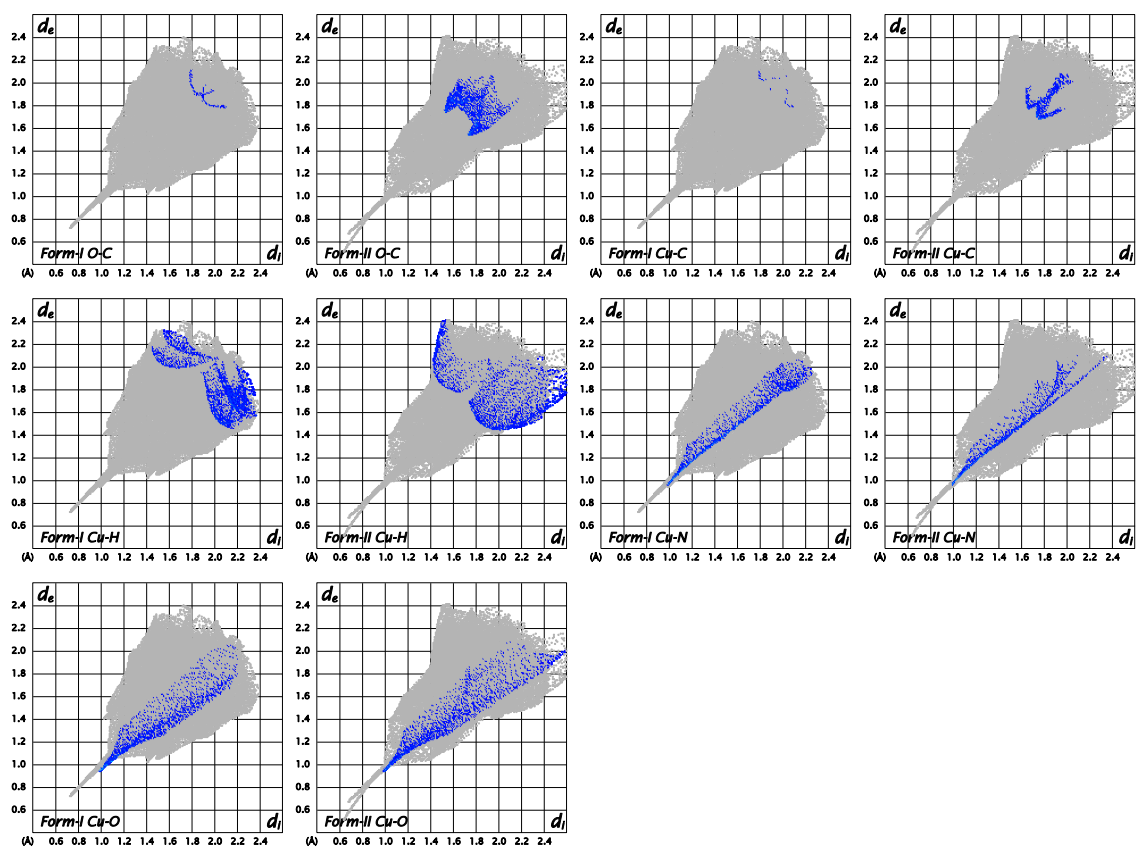


Figure S5. (Continued) Fingerprint plots for form-I and form-II $\text{Cu}_2\text{-TCNQ}$ resolved into individual atomic contacts.

Table S1. Relative contributions to the Hirshfeld surface area for the various close intermolecular contacts for form-I and form-II CuQ₂-TCNQ.

contacts	Form-I (%)	Form-II (%)
H-H	19.6	21.2
H-C	15.0	17.4
H-N	29.8	18.4
H-O	9.3	6.6
H-Cu	3.2	2.9
C-C	13.6	16.4
C-N	3.4	8.1
C-O	0.2	2.5
C-Cu	0.1	1.0
N-N	0.7	0.7
N-O	0.1	0.5
N-Cu	2.7	2.1
O-Cu	2.3	2.2

References:

- ^{s1} Yu, D.H.; Mole, R and Kearley, G. J. European Physical Journal Web of Conferences. **2014**, 83, 03019.
- ^{s2} Yu, D. H.; Mole, R.; Noaks, T.; Kennedy, S. and Robinson, R. J. Phys. Soc. Japan. **2013**, 82, SA027.
- ^{s3} D. Richard, M. Ferrand and G.J. Kearley. J. Neutron Research 4 (1996) 33.
- ^{s4} Furrer, A.; Mesot, J.; and Strässle, T. *Neutron scattering in condensed matter physics*. World Scientific Pub Co Inc, 2009.
- ^{s5} Kresse, G. and Furthmuller, J. Phys. Rev. B **1996**, 54, 11169.
- ^{s6} Kresse, G. and Furthmuller, J. Comput. Mater. Sci. **1996**, 6, 15.
- ^{s7} Blochl, P. E. Phys. Rev. B **1994**, 50, 17953.
- ^{s8} Perdew, J. P.; Burke, K. and Ernzerhof, M. Phys. Rev. Lett. **1997**, 78, 1396.
- ^{s9} Monkhorst, H. J.; Pack, J. D. *Phys. Rev. B* **1976**, 13, 5188.
- ^{s10} Rog, T.; Murzyn, K.; Hinsien, K. and Kneller, G. R. J. Comput. Chem. **2002**, 24, 65721.
- ^{s11} Wolff, S.K.; Grimwood, D. J.; McKinnon, J. J.; Turner, M. J.; Jayatilaka, D.; Spackman, M. A. CrystalExplorer (Version 3.1), University of Western Australia, 2012.
- ^{s12} Spackman, M. A. and McKinnon, J. J. *CrystEngComm*, **2002**, 4, 378.